IEEE Access
Multidisciplinary | Rapid Review | Open Access Journal

Received May 12, 2018, accepted June 5, 2018, date of publication June 11, 2018, date of current version July 19, 2018.

Digital Object Identifier 10.1109/ACCESS.2018.2846293

Insulator Fault Detection Based on Spatial Morphological Features of Aerial Images

YONGJIE ZHAI[1], (Member, IEEE), RUI CHEN[1], QIANG YANG[2], (Senior Member, IEEE), XIAOXIA LI[2], AND ZHENBING ZHAO[1], (Member, IEEE)

[1]Department of Automation, North China Electric Power University, Baoding 071003, China
[2]College of Electrical Engineering, Zhejiang University, Hangzhou 310027, China

Corresponding author: Qiang Yang (qyang@zju.edu.cn)

This work was supported in part by the National Natural Science Foundation of China under Grant 51777183 and Grant 61773160, in part by the Natural Science Foundation of Zhejiang Province under Grant LZ15E070001, in part by the Natural Science Foundation of Jiangsu Province under Grant BK20161142, and in part by the Natural Science Foundation of Hebei Province under Grant F2017502016.

ABSTRACT Because insulators provide electrical insulation and mechanical support for electric transmission lines, these components are of paramount importance to safe and reliable operations of power systems. However, insulators are often considered to be prone to different faults, e.g., bunch-drop, which demands a novel solution for accurate fault detection and fault location. Current research efforts have primarily focused on the bunch-drop fault of glass insulators, and the study of ceramic insulators has not been reported to date. To this end, this paper proposes an algorithmic solution for the bunch-drop fault detection for both glass and ceramic insulators based on spatial morphological features, which can be integrated into an unmanned aerial vehicle-based inspection system. Color models can be established based on the unique color features of both glass and ceramic insulators. Next, the target areas of the insulators can be identified according to the color determination combined with the insulator's spatial features. The target area is morphologically processed to highlight the fault location, and the rules are established based on the spatial feature differences between the insulators with and without faults. Consequently, the fault location can be accurately identified, and the coordinates can be determined. The performance of the proposed solution is evaluated in comparison with existing solutions. The numerical results demonstrate that the proposed solution can detect the bunch-drop faults of insulators with a better than average detection rate. In addition, the performance is assessed and validated in terms of robustness and real-time performance.

INDEX TERMS Bunch-drop, color determination, fault detection, insulator, morphology, spatial features.

I. INTRODUCTION

The insulator is one of the most important components for electrical insulation and mechanical support in electric power transmission lines. Insulators are subjected to large mechanical tension and extremely high voltage with long time exposure outdoors. The defects or faults of insulators can directly lead to significant power loss and can even result in large-scale power outages or blackouts. The insulators that are adopted in transmission lines are primarily made of ceramic and glass. The ceramic insulators are polycrystalline heterogeneous materials, and cracks can occur due to mechanical, electrical and external forces. In the case of strikes due to lightening, an electric arc forms a drainage channel in the head ceramic parts, and the ceramic can burst, which causes a bunch-drop accident. Glass insulators are considered to have uniform texture and compact structure. Although the tensile strength is improved by toughening, a bunch-drop can occur due to overloading. In general, such an insulator fault can be identified visually. However, an assessment method by human visual inspection is inefficient and even not feasible in practice for high-voltage transmission lines that span a large geographical area because of the high error rate and long assessment time. In recent years, the development direction of line inspection has trended toward the use of unmanned aerial vehicle (UVA) inspection. Through the processing and analysis of the aerial images captured by the UAV, the faults in the insulators can be efficiently detected and located [1]–[4].

In the literature, numerous studies have been conducted to address the challenge of insulator fault detection, and a collection of solutions is available. Wang and Yan [5] performed rough segmentation of insulators in a laboratory space to obtain two value images to represent the location and

range of the insulators. A mathematical model was developed to calculate the ratio of the effective pixels in the insulator area for bunch-drop fault detection. In [6]–[8], the identified insulator region was divided into blocks, and insulator bunch-drop fault diagnosis could be conducted using a texture feature quantity. This method performs well in bunch-drop fault diagnosis for the overlapping insulator pieces, but the performance degraded in the cases in which insulator pieces were separated from each other, which could lead to a false diagnosis result. In [9], the insulator region was divided into a flake area based on the insulator string, and the center of gravity of each insulator string was analyzed. The center of gravity distance between the adjacent insulator pieces could be calculated, and hence, the fault location could be determined based on the difference in the center of gravity distance. However, the performance of this solution can be degraded by the background texture and light, and the system might not be able to obtain the complete insulator area. The studies in [10] and [11] adopted the maximum between-cluster variance and the Adaboost classifier to locate the insulator position and then calculate the relative distance of the adjacent insulator piece for bunch-drop fault detection using the insulator contour. This method is merely applicable to the independent and unobstructed situation among adjacent insulators in aerial images. In [12], the proposed solution adopted the color determination method to segment the insulators and locate the defective parts through an adaptive morphology. However, such an approach cannot be applied to ceramic insulators because the ceramic insulators can hardly be identified from the background. In [13] and [14], the sliding window algorithm was developed to match the gray histogram of the template and the captured insulators. The insulator defects can be identified and located based on the distance of the histogram. The performance can be significantly affected by the detection environment and the selection of templates. The studies in [15] and [16] adopted advanced deep learning algorithms (CNN and Faster-RCNN) to identify the location of insulators. However, a large number of image samples and computational time are generally required during the training process, and the on-board GPU is needed to carry out the task. The detection of insulator bunch-drop fault has not been explicitly studied in these studies. Gao *et al.* [17] adopted a deep learning based algorithm (VGG16) to identify insulators from the complex background using pixel reconstruction. However, the detection of insulator string fault was based on conventional method of finding the center of mass, and is limited to the glass insulators.

It can be observed that most existing studies have focused on glass insulators, and it is firmly assumed that the insulators are independent without obstacles. However, because the shooting distance and angle of aerial images vary over time during the UAV inspection, the insulator pieces in the aerial images can be connected and overlapping. It should be highlighted that the ceramic insulators dominate in electric power transmission lines in many cases, and few studies are available for fault detection of ceramic insulators.

Motivated by the existing solutions (e.g., [12], [18]), this paper proposes an algorithmic solution for insulator fault detection that is based on the spatial morphology features of obtained UAV aerial insulator images while considering the unique spatial and color features of glass insulators and ceramic insulators. The basic idea behind the proposed algorithmic solution is illustrated in Fig. 1 and summarized as follows: the color model for image segmentation is established based on the color features of glass and ceramic insulators. The captured insulators with different angles can be processed using the Hough Transform to detect the straight lines, and the insulators can be located. Finally, the located insulator is processed through morphological processing, and the spatial features of the fault location are analyzed; subsequently, the rules can be established. Based on these rules, the fault location coordinates in the insulators can be determined.

In summary, the main technical contributions made in this work can be summarized as follows: (1) the proposed solution can accurately identify and locate the bunch-drop faults based on the spatial features of UAV aerial images of both glass and ceramic insulators; and (2) the robustness and real-time performance of the proposed solution is evaluated and validated. The numerical result demonstrates that the proposed solution outperforms the existing solutions.

The remainder of this paper is organized as follows: Section II presents the insulator target detection process. Section III presents the detection and location method of the insulator bunch-drop fault in detail. Section IV reports on a range of experiments that were performed and presents the numerical results. Finally, the study's conclusions are presented in Section V.

II. INSULATOR TARGET DETECTION

A. COLOR DETERMINATION

The color histogram was first used for image feature extraction in [19] and is considered to be an efficient method for describing the color features. The histogram can well reflect the composition and distribution of the image colors, i.e., the probability of the appearance of various colors. In [20] and [21], the Lab color space or HIS color space was used to distinguish the glass insulators based on the empirical threshold. However, it should be noted that the segmentation of insulators from the complex background can be hardly

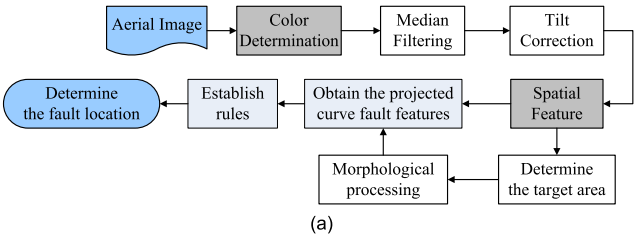

FIGURE 1. Flowchart of the proposed fault detection method. (a) Overall process of the algorithmic solution.

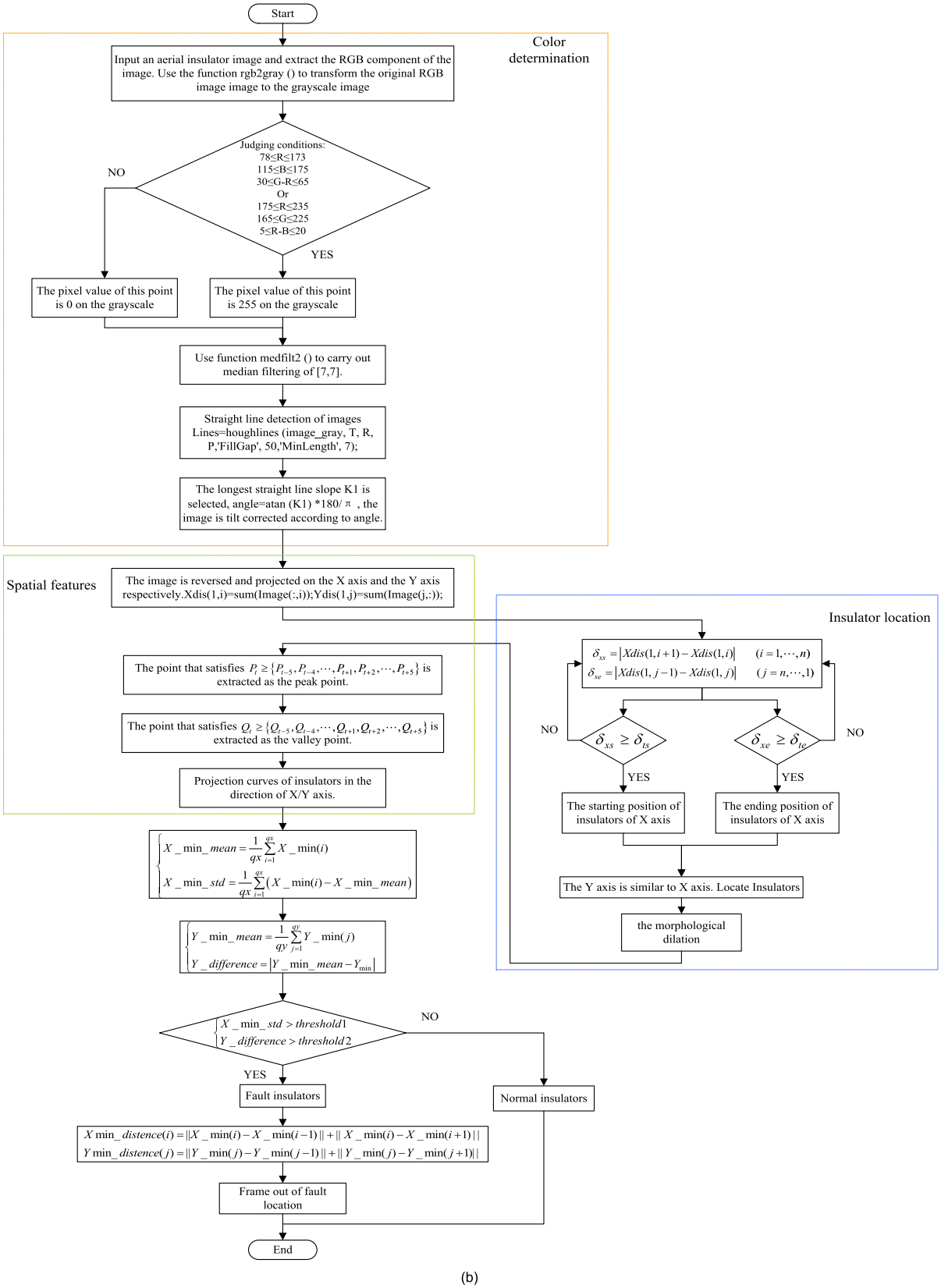

(b)

FIGURE 1. *(Continued.)* **Flowchart of the proposed fault detection method. (b) Detailed flowchart of the proposed algorithmic solution.**

achieved by the use of one threshold in practice. In addition, most of the solutions have merely focused on the glass insulators, and little investigation has been made of ceramic insulators. To accomplish this goal, this work exploits both types of insulators (i.e., glass and ceramic), and obtains the color distribution by sampling the RGB values of 100 glass insulators and ceramic insulators, as shown in Fig. 2.

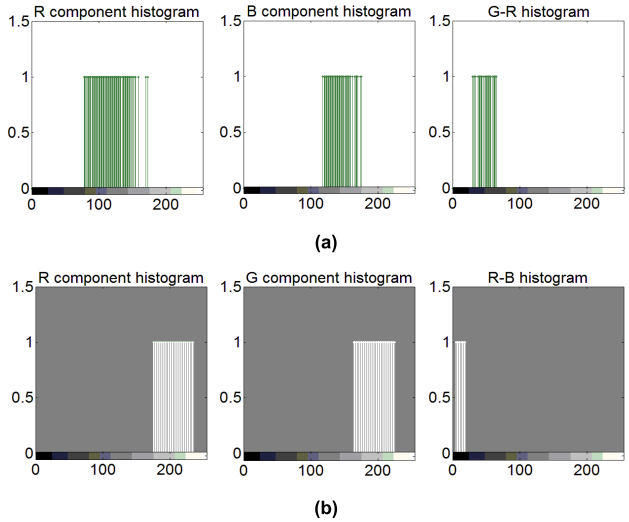

FIGURE 2. Histogram distribution of two material insulators in RGB color space. (a) Distribution histogram of glass insulators in RGB color space. (b) Distribution histogram of ceramic insulators in RGB color space.

Based on the unique distribution of glass insulators and ceramic insulators in RGB color space, the insulator can be effectively identified from the background by setting corresponding thresholds for the R (red), G (green) and B (blue) color components. The color distributions of the glass and ceramic insulators are expressed in (1) and (2), respectively.

$$\begin{cases} 78 \le R \le 173 \\ 115 \le B \le 175 \\ 30 \le G - R \le 65 \end{cases} \tag{1}$$

$$\begin{cases} 175 \le R \le 235 \\ 165 \le G \le 225 \\ 5 \le R - B \le 20 \end{cases} \tag{2}$$

The pseudo-code of color determination process for glass insulators is presented in Algorithm 1.

This color model can segment the insulator region from the complex background. The segmentation results of the glass and ceramic insulators are presented in Fig. 3.

B. NOISE FILTERING AND TILT CORRECTION

The insulator image can be segmented from the complex background based on color features, but when there is noise, it deteriorates the image quality for further analysis. In this instance, the median filter [22] is adopted to filter the lone noise while maintaining the edges of the images based on a nonlinear signal processing technique. Simultaneously,

Algorithm 1: Color Determination of Glass Insulators

Input: *image*
Output: *image_gray*

$R = image(:, :, 1), G = image(:, :, 2),$
$B = image(:, :, 3)$
$[m, n] = size(image)$
$image\_gray = rgb2gray(image)$
for $i = 1$ *to* m **do**
  for $j = 1$ *to* n **do**
    $R = image(i, j, 1), G = image(i, j, 2), B = image(i, j, 3)$
    $bool_1 = (78 \le R \le 173), bool_2 = (115 \le B \le 175),$
    $bool_3 = (30 \le G - R \le 65)$
    if $bool_1$ *and* $bool_2$ *and* $bool_3$ **then**
      $image_gray(i, j) = 255$
    else
      $image_gray(i, j) = 0$
    end if
  end for
end for

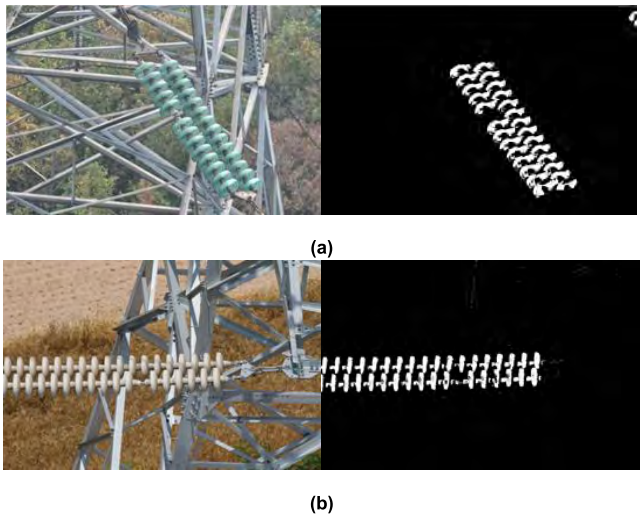

FIGURE 3. Results of color determination. (a) The segmentation results for the glass insulator. (b) The segmentation results for the ceramic insulator.

it also calculates the connected domain of the filtered image, removes the smaller part of the connected domain, and further strengthens the target area. The results of the process are presented in Fig. 4.

In reality, because the insulator images are often captured with different angles during inspection, the Hough transformation [23] is adopted to detect the straight lines, as well as to correct the images, thereby facilitating the follow-up operation, as shown in Fig. 5. The target image can be identified using the line detection of the Hough transformation, and the location of the longest line segment is obtained. In light of the slope of the straight line, the angle of the insulator is

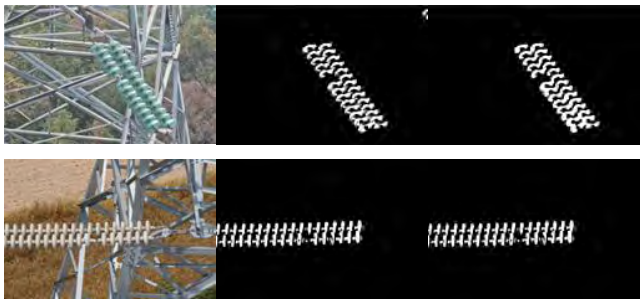

FIGURE 4. Noise filtering process. (a) Original image. (b) Median filter. (c) Removal of the smaller part of the connected domain.

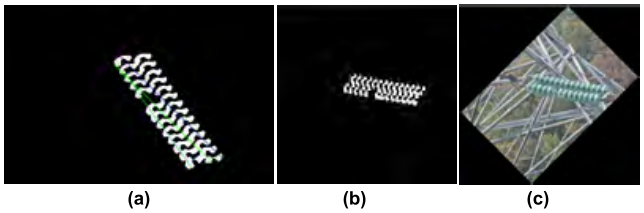

FIGURE 5. Tilt correction. (a) Hough transformation detection of lines. (b) Tilt correction. (c) Correction of original image.

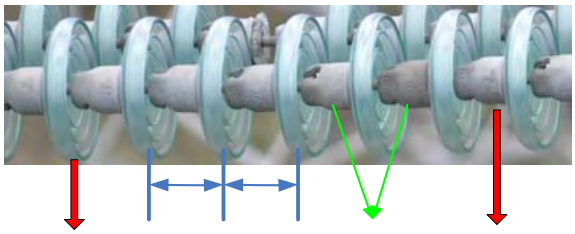

FIGURE 6. Structure of the insulator.

determined, and then, the target image is rotated to perform a tilt correction.

C. SPATIAL FEATURES OF INSULATORS

Fig. 6 illustrates the structure and components of the insulator. The insulator is composed of a vertical arrangement along the center axis and a number of insulator pieces that have the same shape and color, which indicates consistency in the form of space [18].

To clearly observe the insulator features, the reverse operation of the insulator image is conducted through a tilt correction. The pseudo-code of spatial feature analysis is presented in Algorithm 2.

Fig. 7 shows the projection on the X axis and Y axis. Based on the projection curves in the X/Y axis, the peak number n_v and valley number m_v can be determined as follows: The point P_t that satisfies formula (3) is extracted as the peak point. In this case, there can be multiple adjacent peak points in the horizontal curve segment, and we extract the intermediate point as the peak point. The number of peak points is counted

Algorithm 2: Spatial Features of Insulators in the Direction of X Axis

Input: src

Output: $figure$

Require: $X_{dis}, X_{max}, X_{min}, X_{maxx}, X_{minx}, X_m, X_i$, $p_x = 0; q_x = 0; t_r = 1, t_x = 1$

```
src = im2bw(src, 0.5)
src =~ src
[m, n] = size(src)
for i = 1 to n do
    X_dis(1, i) = sum(src(:, i))
end for
for t = 5 to n − 6 do
    if X_dis(1, t − 4 : t − 1) ≤ X_dis(1, t) ≤ X_dis(1, t + 4 : t + 1)
    then
    t_r = t_r + 1, X_m(1, t_r) = t
    if X_m(1, t_r) > X_m(1, t_r − 1) + 2 then
        p_x = p_x + 1, X_max(1, p_x) = X_dis(1, t), X_maxx(1, p_x) = t
    end if
  else
    tx = tx + 1, X_i(1, t_x) = t
    if X_m(1, t_r) > X_m(1, t_r − 1) + 2 then
        q_x = q_x + 1, X_min(1, q_x) = X_dis(1, t), X_minx(1, q_x) = t
    end if
  endif
end for
figure : plot(1 : n, Xdis), plot(X_maxx, X_max),
plot(X_minx, X_min)
```

which is denoted as n_v.

$$P_t \geq \{P_{t-5}, P_{t-4}, \cdots, P_{t+1}, P_{t+2}, \cdots, P_{t+5}\} \quad (3)$$

where $t = 6, 7, \cdots, G_w - 5$, G_w is the width of the insulator target area, and P_t is the peak projection value.

Similarly, the point Q_t that satisfies formula (4) is extracted as the valley point. In the case in which there exist multiple adjacent valley points in the horizontal curve segment, the intermediate point is extracted as the valley point. The number of valley points is counted and is denoted as m_v.

$$Q_t \geq \{Q_{t-5}, Q_{t-4}, \cdots, Q_{t+1}, Q_{t+2}, \cdots, Q_{t+5}\} \quad (4)$$

where $t = 6, 7, \cdots, G_w - 5$, G_w is the width of the insulator target area, and Q_t is the valley projection value.

It can be observed from the projection curves that the insulator projection curves exhibit obvious regular features.

The projection curves in the direction of the X axis are mostly equal amplitude oscillations. Each peak corresponds to an insulator piece, and the valley corresponds to the center of the steel cap. The distance between the peak and valley alternately appears which corresponds to the isometric arrangement of the insulator pieces. In addition, the projection curve in the direction of the Y axis is a single peak curve

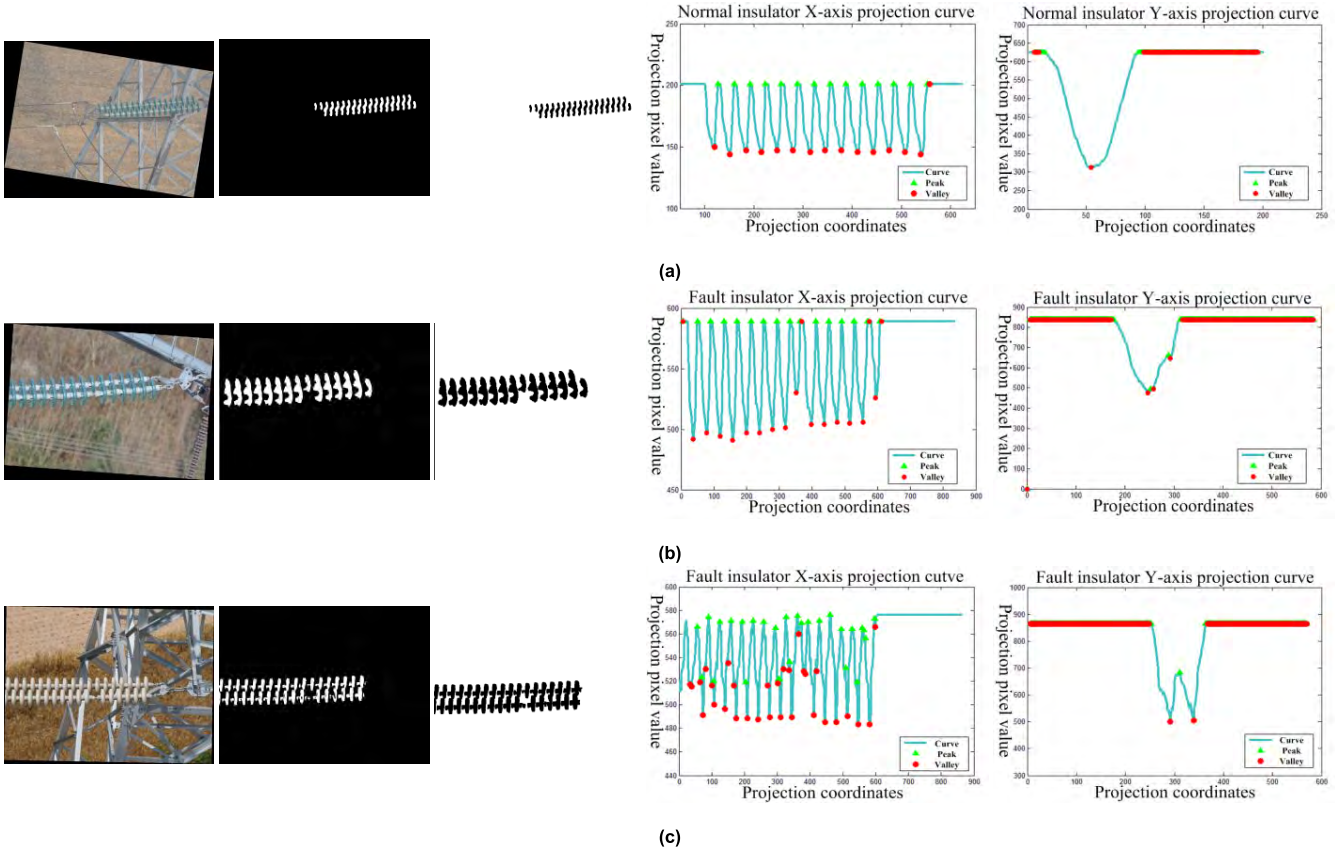

FIGURE 7. Projection curves of insulators in the direction of X/Y axis. (a) Projection curves of normal insulator in the direction of X/Y axis. (b) Projection curves of fault glass insulator in the direction of X/Y axis. (c) Projection curves of fault ceramic insulator in the direction of X/Y axis.

that has a certain width. In fact, the position of the wave peak corresponds to the center axis of the insulator.

D. LOCATE INSULATORS

Based on the spatial features, the insulator can be located using its projection curve through the following steps:

Step #1: the insulator position in the X axis must be determined first. It can be seen from the projection curve that the position of the insulator in the X axis is the position of its projection curve of the constant amplitude oscillation portion in the X axis. Therefore, the difference in the projection value of the adjacent position is obtained by formula (5), and when it is larger than the set threshold, it is determined to be the starting position. The difference in the projection value of the adjacent position is obtained by the reverse formula (6), and it exceeds the pre-defined threshold; it is considered to be the termination position.

$$\delta_{xs} = |Xdis(1, i+1) - Xdis(1, i)| \quad (i = 1, \cdots, n) \quad (5)$$

$$\delta_{xe} = |Xdis(1, j-1) - Xdis(1, j)| \quad (j = n, \cdots, 1) \quad (6)$$

where n is the horizontal size of the image; and $Xdis$ is the projection value of the image in the direction of the X axis.

Step #2: determination of the insulator position in the Y axis, which is similar to step #1.

Step #3 determination of the insulator location in accordance with the position coordinates obtained by steps (1) and (2).

Finally, the experimental result clearly demonstrates the accuracy of the insulator location, as presented in Fig. 8.

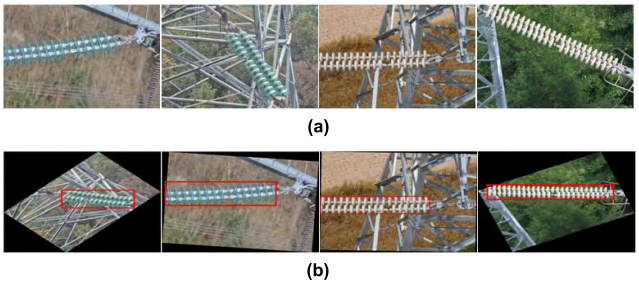

FIGURE 8. The results of locating the insulator. (a) Original images. (b) Located images.

III. INSULATOR BUNCH-DROP DETECTION AND LOCATION

For insulators, the spacing between adjacent insulator pieces is equal. After a bunch-drop occurs, the width of the adjacent insulator pieces will become significantly larger. A clear gap in the insulator area can be observed by human visual inspection. Upon determining the location of the insulators,

the morphological algorithm [24] is adopted to highlight the location of the missing piece, such that the fault position can be detected and located through its spatial features.

A. MORPHOLOGICAL PROCESSING

Mathematical morphology is an efficient image analysis method based on lattice and topology, which uses the fundamental morphological transformations, e.g., dilation and erosion. A variety of functions can be conducted to eliminate noise, separate independent image elements, and connect adjacent elements in the image. To highlight the position of the insulator bunch-drop, the morphological dilation is adopted to narrow the gap between the normal insulator pieces and to keep off the bunch-drop spacing. The processing results using morphological dilation are illustrated in Fig. 9.

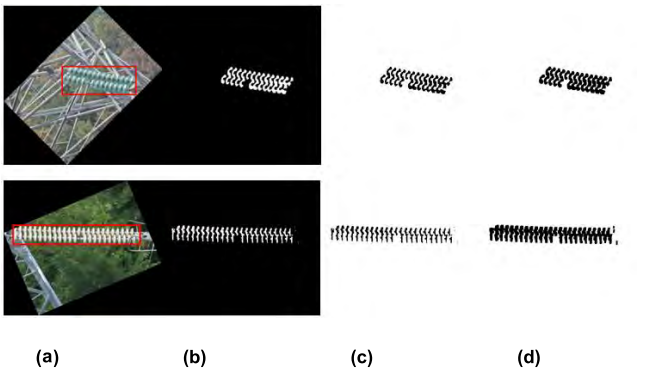

FIGURE 9. The result of morphological dilation processing. (a) Insulator image. (b) Color determination. (c) Reverse operation. (d) Dilation processing.

B. SPATIAL FEATURES OF INSULATOR BUNCH-DROP

The morphological dilation insulator image is spatially projected. Next, it can be seen that when the insulator bunch-drop occurs, there is a significant difference in the projection between normal insulators and fault insulators, as shown in Fig. 10. Through examining the projection curves for normal and fault insulators, it can be found that the distribution of the peak and valley values of normal insulators is relatively uniform in the X axis, while the valley values of the fault insulators are obviously changed. In the Y direction, the projection curve of the normal insulators is smooth, and the projection curve of the fault insulators has obvious protrusions.

C. INSULATOR BUNCH-DROP DETECTION AND LOCATION

1) DETECTION

From the projection curve analysis of both normal insulators and fault insulators, the following phenomenon can be observed: upon the occurrence of a fault in an insulator, the valley value of the X-axis projection curve will jump, and the valley value (excluding the valley maximum) of the Y-axis projection curve there will be a new mutation. Therefore, the fault identification in an insulator can be conducted

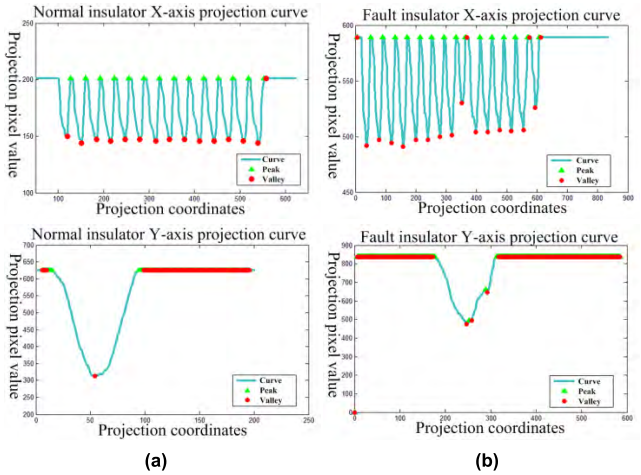

FIGURE 10. Normal insulator and fault insulator projection comparison image. (a) Normal insulator projection curve. (b) Fault insulator projection curve.

through calculating the variance of the valley value in the X-axis and the average of the valley value while excluding the valley maximum value in the Y-axis. In the case in which the variance $X\_\min\_std$ of the valley on the X-axis is larger than that of a predefined threshold ($thd_1 = 10$) and the difference $Y\_difference$ between the valley value and the minimum valley value on the Y-axis is larger than a predefined threshold ($thd_2 = 2$), the insulator is considered to have a fault.

$$\begin{cases} X\_\min\_mean = \dfrac{1}{q_x}\displaystyle\sum_{i=1}^{q_x} X\_\min(i) \\ X\_\min\_std = \dfrac{1}{q_x}\displaystyle\sum_{i=1}^{q_x} (X\_\min(i) - X\_\min\_mean) \end{cases} \tag{7}$$

$$\begin{cases} Y\_\min\_mean = \dfrac{1}{q_y}\displaystyle\sum_{j=1}^{q_y} Y\_\min(j) \\ Y\_difference = |Y\_\min\_mean - Y_{\min}| \end{cases} \tag{8}$$

where q_x is the number of valleys on the X-axis direction projection curve; $X\_\min(i)$ is the pixel value of the i^{th} valley on X-axis projection curve; q_y is the number of valleys on Y-axis projection curve (remove the valley maximum); $Y\_\min(j)$ is the pixel value of the j^{th} valley on the Y-axis direction projection curve; and $Y_{\min}$ is the valley minimum on the Y-axis direction projection curve.

2) LOCATION

After the morphological dilation, the gap in the fault area is highlighted when a bunch-drop fault occurs. Therefore, the bunch-drop faults can be located by the spatial features in the following steps:

(1) The X-axis coordinate determination of the bunch-drop fault: Based on the fault's X-axis direction projection, the mutation position of the valley can be identified. All of the valley values are sorted in the X-axis direction

in descending order; the valley that corresponds to the maximum value of the distance difference can be found using (9), and the X-coordinate of the valley is used as the X-axis coordinate;

$$X\_min\_distence(i) = \|X\_min(i) - X\_min(i-1)\| + \|X\_min(i) - X\_min(i+1)\| \quad (9)$$

where i represents the i^{th} valley point;

(2) The Y-axis coordinate determination of the bunch-drop fault. The process is similar to the determination of the X-axis coordinate, and (10) is adopted.

$$Y\_min\_distence(j) = \|Y\_min(j) - Y\_min(j-1)\| + \|Y\_min(j) - Y\_min(j+1)\| \quad (10)$$

where j denotes the j^{th} valley;

(3) Finally, the position of the bunch-drop fault is determined. Based on the obtained coordinates of the X-axis and Y-axis, a square with a predefined threshold ($thd_3 = 40$) is used. The identified location is illustrated in Fig. 11.

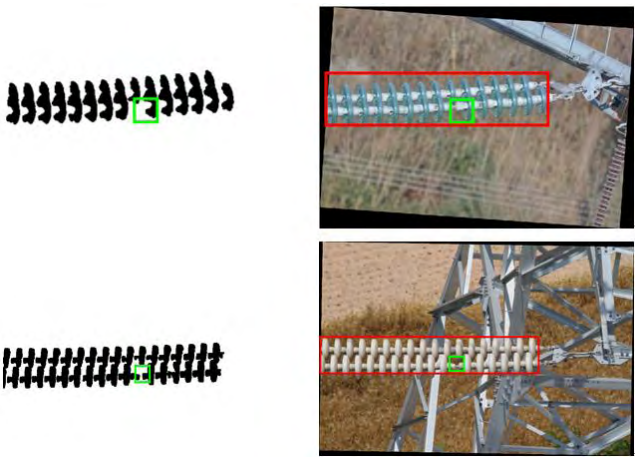

FIGURE 11. Images of located insulator.

IV. EXPERIMENTAL RESULTS AND ANALYSIS

A. EXPERIMENTAL RESULTS

The proposed solution is expected to detect and locate, in a timely and accurate manner, the insulator bunch-drop fault in the context of a complex background captured using an UAV. This section extensively evaluates the proposed solution using collected aerial images based on a UAV inspection system of electric transmission lines in the field. The effectiveness and performance of the insulator bunch-drop fault detection is evaluated, and the analysis solution is implemented and validated. The experimental environment is established based on the Windows 7 operating system, MATLAB R2014a and Microsoft Visual Studio 2010, and the CPU main frequency and memory are 2.50 GHz and 4.00 GB, respectively.

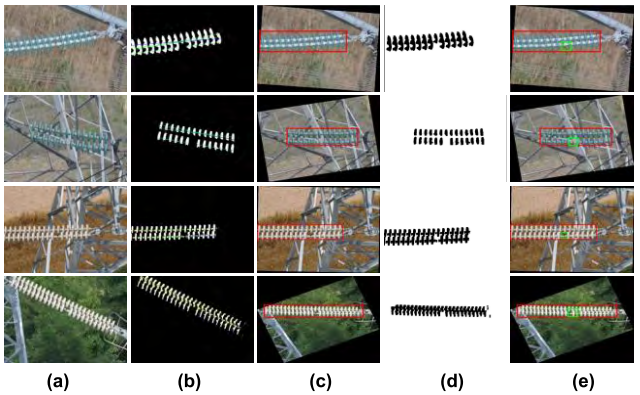

FIGURE 12. Experimental results. (a) Original image; (b) Tilt correction image; (c) Located insulator image; (d) Morphological dilation image; and (e) Located image of insulator with fault.

Fig. 12 presents a collection of experimental results, including the original images, tilt correction image, located insulator image, and morphological dilation image, as well as the final located image of the insulator with the fault. The result clearly confirms that the proposed solution can efficiently identify and locate the insulators that have bunch-drop faults.

B. ROBUSTNESS ANALYSIS

In this analysis, the robustness of the proposed solution is exploited through a comparative study with the existing insulator bunch-drop detection solutions.

1) FAULT FEATURES HAVE OCCLUSION

In reality, the captured aerial insulator images using a UAV often have shadows between the insulator pieces. In this case, the adjacent insulator pieces are stuck to each other, and the boundary between the insulators becomes unclear. It is difficult to judge the specificities of the individual insulator pieces' positions, which results in a higher false detection rate. The robustness of the proposed solution in this work is evaluated against the solutions presented in [8] and [14] for the obtained aerial images with different shooting angles. The experimental results are presented in Figs. 13 and 14. It can be observed that the proposed algorithm can accurately locate the bunch-drop faults in both cases and clearly indicate that the proposed solution based on the spatial morphological features has sufficient robustness.

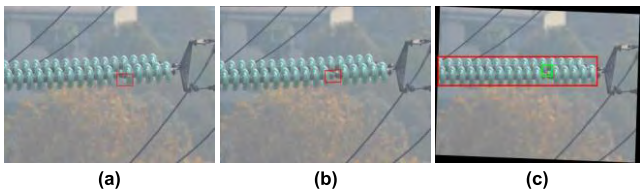

FIGURE 13. Detection results of insulators without occlusions. (a) Method [8]; (b) Method [14]; (c) Proposed method.

FIGURE 14. Detection results of insulators with an occlusion. (a) Method [8]; (b) Method [14]; (c) Proposed method.

2) DIFFERENT BACKGROUND AND SHOOTING DISTANCES

In addition, the performance of the proposed solution is further evaluated based on the UAV captured images shot with different backgrounds and distances. The experimental results under the condition of a simple background and a complex background are provided in Figs. 15 and 16, respectively. It is demonstrated that the proposed solution can obtain robust detection and diagnostic results using the captured images from different shooting situations.

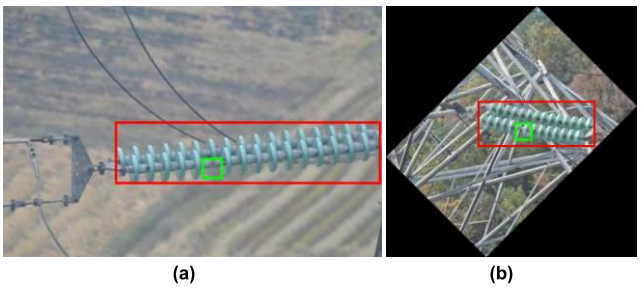

FIGURE 15. Experimental results under different backgrounds. (a) Aerial image in a simple background; (b) Aerial image in a complex background.

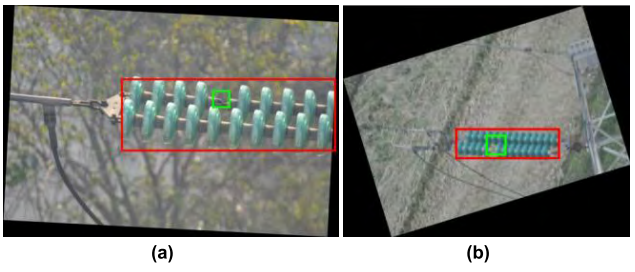

FIGURE 16. Experimental results of different shooting distances. (a) Close-up shot image; (b) Long-range shot image.

3) INSULATORS OF DIFFERENT MATERIALS

Most of the available insulator bunch-drop fault detection solutions are designed for glass insulators, and hence, they cannot be directly adopted for ceramic insulators. In this study, the proposed algorithmic solution can be applied to both glass and ceramic insulators. The experimental results for the fault detection of ceramic insulators are shown in Fig. 17. These results demonstrate that the proposed solution is efficient for fault detection in ceramic insulators.

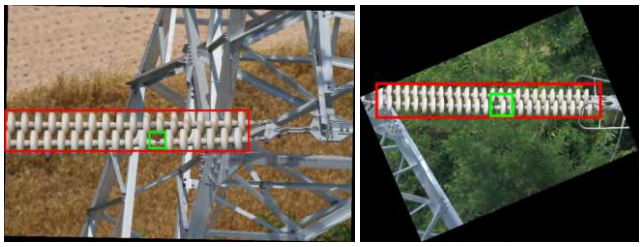

FIGURE 17. Bunch-drop fault detection in ceramic insulators.

TABLE 1. Comparison of the time consumption and detection rate of the algorithms.

Algorithms	Insulator type	Average time consumption/s	Detection success rate
literature [5]	Glass	1.957	65.4%
	Ceramic	—	—
literature [12]	Glass	0.525	92.4%
	Ceramic	—	—
Proposed Algorithm	Glass	0.677	92.8%
	Ceramic	0.677	90.6%

C. REAL TIME PERFORMANCE AND DETECTION RATE

Finally, the real-time performance and detection success rates of the proposed solution are analyzed through the detection of 74 bunch-drop insulator images (glass samples: 42, ceramic samples: 32), each of which contains one bunch-drop fault. The efficiency the proposed solution is evaluated through examining the average time consumed in the fault detection process, as well as the bunch-drop fault detection success rate. The performance of the proposed algorithmic solution is evaluated in comparison with the solutions proposed in [5] and [12], and the numerical results are presented in Table 1. It can be observed that the proposed solution outperforms the solution in [5] with significantly reduced average consumed time for the fault detection and an improved detection success rate. It is also shown that the proposed solution provides similar performance to the solution proposed in [12], with a slightly longer average detection time, but a better detection success rate. It should be noted that the solutions in both [5] and [12] can only conduct fault detection for glass insulators and are not applicable for ceramic insulators. The proposed solution in this work can be used for fault detection of both glass and ceramic insulators, and the performance results for ceramic insulators are provided in Table 1. The numerical result clearly confirms the real-timeliness (0.667s on average) and accuracy (success rate of 90.6%) of the proposed solution for fault detection of ceramic insulators.

V. CONCLUSIONS AND FUTURE WORK

In this paper, a novel algorithmic solution for bunch-drop fault detection and location determination for both glass and ceramic insulators based on the spatial morphological features is proposed. The proposed solution can efficiently identify both glass and ceramic insulators from UAV captured

aerial images with complex background based on spatial features. Afterward, the target area can be morphologically processed to highlight the fault's position. As a result, the fault insulators can be identified and located based on the spatial features. The performance of the proposed solution is extensively evaluated for a range of scenarios. The experimental results confirm its effectiveness and robustness as well as its real-timeliness. The average fault detection success rate in ceramic can reach over 91%, while the average fault detection success rate of glass can reach over 92%. As a result, the proposed solution can be adopted in the inspection system of large-scale infrastructures, e.g., high-voltage transmission lines of power utilities.

The proposed solution is able to locate the ceramic insulators and glass insulators, but the automatic differentiation of insulator types is not implemented. Also, the size of the fault area in insulators cannot be accurately obtained during the fault detection process in the proposed solution. Therefore, a number of research directions are considered worth further research effort. Firstly, more advanced approach is needed to efficiently distinguish different types of insulators for fault detection and analysis. Secondly, as the performance of insulator identification merely based on the color features can significantly degrade in the presence of complex background, more advanced image segmentation algorithms and tools need to be further studied. Finally, additional work is needed for location and detection of multiple simultaneous bunch-drop faults in insulators based on spatial features.

REFERENCES

[1] S. P. Zhang, Z. Yang, X. N. Huang, and Y. Z. Wu, "Defects detection and positioning for glass insulator from aerial images," *J. Terahertz Sci. Electron. Inf. Technol.*, vol. 11, no. 4, pp. 609–613, Aug. 2013.

[2] T. Hirakawa *et al.*, "Tree-wise discriminative subtree selection for texture image labeling," *IEEE Access*, vol. 5, pp. 13617–13634, Jul. 2017.

[3] L. Li, L. Sun, W. Kang, J. Guo, C. Han, and S. Li, "Fuzzy multilevel image thresholding based on modified discrete grey wolf optimizer and local information aggregation," *IEEE Access*, vol. 4, pp. 6438–6450, Sep. 2016.

[4] Z. Guan, X. Wang, X. Bian, L. Wang, and Z. Jia, "Analysis of causes of outdoor insulators damages on HV and UHV transmission lines in China," in *Proc. IEEE Elect. Insulation Conf. (EIC)*, Philadelphia, PA, USA, Jun. 2014, pp. 227–230.

[5] Y. L. Wang and B. Yan, "Vision based detection and location for cracked insulator," *Comput. Eng. Des.*, vol. 35, no. 2, pp. 583–587, Feb. 2014.

[6] D. Zuo, H. Hu, R. Qian, and Z. Liu, "An insulator defect detection algorithm based on computer vision," in *Proc. IEEE Int. Conf. Inf. Automat. (ICIA)*, Macau, China, Jul. 2017, pp. 361–365.

[7] J. Han, J. J. Zhang, and B. H. Wang, "Method on recognizing the structure of transmission line based on perceptual organization," *Infrared Laser Eng.*, vol. 42, no. 12, pp. 3458–3463, Dec. 2013.

[8] W. Wang, Y. Wang, J. Han, and Y. Liu, "Recognition and drop-off detection of insulator based on aerial image," in *Proc. 9th Int. Symp. Comput. Intell. Design (ISCID)*, Hangzhou, China, 2016, pp. 162–167.

[9] Y. T. Jiang *et al.*, "The identification and diagnosis of self-blast defects of glass insulators based on multi-feature fusion," *Electr. Power*, vol. 50, no. 5, pp. 52–58, May 2017.

[10] J. P. Shang, C. X. Li, and L. Chen, "Location and detection for self-explode insulator based on vision," *J. Electron. Meas. Instrum.*, vol. 31, no. 6, pp. 844–849, Jun. 2017.

[11] F. Y. Zhang, "Recognition and research of anomaly map of transmission line inspection based on computer vision," M.S. thesis, Dept. Comput., Eng., Jilin Univ., Jilin, China, 2015.

[12] Y. Zhai, D. Wang, M. Zhang, J. Wang, and F. Guo, "Fault detection of insulator based on saliency and adaptive morphology," *Multimedia Tools Appl.*, vol. 76, no. 9, pp. 12051–12064, May 2017.

[13] L. Shi, "The method of image detection on defect insulator in transmission line," M.S. thesis, Dept. Control. Eng., North China Electric Power Univ., Beijing, China, 2013.

[14] F. Gao *et al.*, "Recognition of insulator explosion based on deep learning," in *Proc. 14th Int. Comput. Conf. Wavelet Act. Media Technol. Inf. Process. (ICCWAMTIP)*, Chengdu, China, 2017, pp. 79–82.

[15] Y. Liu, J. Yong, L. Liu, J. Zhao, and Z. Li, "The method of insulator recognition based on deep learning," in *Proc. 4th Int. Conf. Appl. Robot. Power Ind. (CARPI)*, Jinan, China, 2016, pp. 1–5.

[16] Z. Zhao, G. Xu, Y. Qi, N. Liu, and T. Zhang, "Multi-patch deep features for power line insulator status classification from aerial images," in *Proc. Int. Joint Conf. Neural Netw. (IJCNN)*, Vancouver, BC, USA, 2016, pp. 3187–3194.

[17] F. Gao, J. Wang, Z. Kong, J. Wu, and N. Feng, "Recognition of insulator explosion based on deep learning," in *Proc. 14th Int. Comput. Conf. Wavelet Act. Media Technol. Inf. Process. (ICCWAMTIP)*, Chengdu, China, 2017, pp. 79–82.

[18] Y. J. Zhai, D. Wang, Z. B. Zhao, and H. Y. Cheng, "Insulator string location method based on spatial configuration consistency feature," *Chin. Soc. Elect. Eng.*, vol. 37, no. 5, pp. 1568–1577, Mar. 2017.

[19] M. J. Swain and D. H. Ballard, "Color indexing," *Int. J. Comput. Vis.*, vol. 7, no. 1, pp. 11–32, 1991.

[20] T. Fang, C. Dong, X.-L. Hu, and Y. Wang, "Contour extraction and fault detection of insulator strings in aerial images," *J. Shanghai Jiaotong Univ.*, vol. 47, no. 12, pp. 1818–1822, Dec. 2013.

[21] C. Yao, L.-J. Jin, and S.-J. Yan, "Recognition of insulator string in power grid patrol images," *J. Syst. Simul.*, vol. 24, no. 9, pp. 1818–1822, Sep. 2012.

[22] K. B. Cui, "Research on the key technologies in insulator defect detection based on image," Ph.D. dissertation, Dept. Elect. Eng., North China Electric Power Univ., Beijing, China, 2016.

[23] X. Y. Zhang, J. B. An, and F. M. Chen, "A method of insulator fault detection from airborne images," in *Proc. 2nd WRI Global Congr. Intell. Syst.*, Wuhan, China, USA, 2010, pp. 200–203.

[24] R. C. Gonzalez, R. E. Woods, and S. L. Eddins, *Digital Image Processing Using MATLAB*. Beijing, China: PHEI, 2013.

YONGJIE ZHAI was born in Luohe, Henan, China, in 1972. He received the B.Sc. degree in automation and the Ph.D. degree from North China Electric Power University. He is currently an Associate Professor with the Department of Automation, North China Electric Power University. His current research focuses on the application of machine learning and image processing in power systems.

RUI CHEN received the bachelor's degree in measurement and control technology and instrument from North China Electric Power University, Baoding, China, in 2016, where she is currently pursuing the master's degree in pattern recognition with the Department of Automation. She is also with the Intelligent System Laboratory. Her area of interest lies on the insulators recognition, fault detection of transmission line, and image processing.

QIANG YANG (M'07–SM'18) received the B.S. degree (Hons.) in electrical engineering, and the M.Sc. (Hons.) and Ph.D. degrees in electronic engineering and computer science from the Queen Mary College, University of London, London, U.K., in 2003 and 2007, respectively. He was a Post-Doctoral Research Associate with the Department of Electrical and Electronic Engineering, Imperial College London, U.K., from 2007 to 2010, where he was involved in a number of high-profile U.K. EPSRC and European IST research projects. He visited The University of British Columbia and the University of Victoria, Canada, as a Visiting Scholar, in 2015 and 2016, respectively. He is currently an Associate Professor with the College of Electrical Engineering, Zhejiang University, China. He has published over 140 technical papers, applied 50 national patents, and co-authored two books and 10 book chapters. His research interests over the years include communication networks, smart energy systems, and large-scale complex network modeling, control, and optimization. He is a member of IET and IEICE, and a Senior Member of the China Computer Federation.

XIAOXIA LI received the bachelor's degree in automation with the College of Electrical Engineering, Zhejiang University, Hangzhou, China, in 2015, where she is currently pursuing the Ph.D. degree in control theory and control engineering. Her research interests include pattern recognition, artificial intelligence, renewable energy analysis, and fault detection using unmanned aerial vehicles.

ZHENBING ZHAO was born in Suqian, Jiangsu, China, in 1979. He received the B.S., M.S., and Ph.D. degrees from North China Electric Power University, Baoding, in 2002, 2005, and 2009, respectively. He is currently an Associate Professor with the School of Electrical and Electronic Engineering, North China Electric Power University. His research interests include machine learning, image processing, and the intelligent detection of electrical equipment.